INTERNATIONAL JOURNAL FOR NUMERICAL METHODS IN ENGINEERING
Int. J. Numer. Meth. Engng 2005; **64**:125–142
Published online 11 July 2005 in Wiley InterScience (www.interscience.wiley.com). DOI: 10.1002/nme.1391

Response surface approach to aerodynamic optimization design of helicopter rotor blade

Hyosung Sun[‡] and Soogab Lee[*, †]

School of Mechanical and Aerospace Engineering, Seoul National University, Seoul 151-742, Korea

SUMMARY

This paper describes a hovering rotor blade design through the suitable combination of flow analysis and optimization technique. It includes a parametric study concerned with the influence of design variables and different design conditions such as objective functions and constraints on the rotor performance. Navier–Stokes analysis is employed to compute the hovering rotor performance in subsonic and transonic operating conditions. Response surface method based on D-optimal 3-level factorial design and genetic algorithm are applied to obtain the optimum solution of a defined objective function including the penalty terms of constraints. The designs of the rotor airfoil geometry and the rotor tip shape are performed in subsonic and transonic conditions, and it is observed that the new rotor blades optimized by various objective functions and constraints have better aerodynamic characteristics than the baseline rotor blade. The influence of design variables and their mutual interactions on the rotor performance is also examined through the optimization process. Copyright © 2005 John Wiley & Sons, Ltd.

KEY WORDS: response surface method (RSM); genetic algorithm (GA); multi-disciplinary design optimization (MDO); analysis of variance; regression analysis

INTRODUCTION

Many researches were conducted to demonstrate the influence of rotor blade geometry parameters such as twist, taper ratio, point of taper initiation, sweep, point of sweep initiation, and airfoil sections on the aerodynamic performance of the rotor blade [1]. However, the influence of geometrical design variables and their interactions on the rotor aerodynamic performance was not examined in detail in these works. From this point of view, the present research is

*Correspondence to: Soogab Lee, School of Mechanical and Aerospace Engineering, Seoul National University, San 56-1, Shinlim-dong, Kwanak-gu, Seoul 151-742, Korea.
†E-mail: solee@plaza.snu.ac.kr
‡E-mail: aerosun@snu.ac.kr

Contract/grant sponsor: Ministry of Science and Technology, Korea
Contract/grant sponsor: Korea Aerospace Research Institute (KARI)

Received 4 March 2004
Revised 9 December 2004
Accepted 21 April 2005

focused on suggesting a rotor blade shape design using the numerical optimization method coupled with the statistical approach. The comparative significance of each design parameter on the rotor performance is also measured, because it can give useful information about the rotor blade design.

The optimization techniques have been studied for the application to the rotor blade design process [2, 3]. Most optimization procedures have dealt with a single discipline such as aerodynamics [4], structures [5], or dynamics [6]. However, the rotor blade design process is multi-disciplinary involving the couplings and interactions between several disciplines such as aerodynamics, dynamics, structures, and acoustics. The techniques and strategies for merging disciplines to obtain integrated rotorcraft optimization procedures have been developed [7, 8]. Many optimization design methods which have peculiar characteristics have shown the advanced features in the rotor blade design at various operating conditions, and this paper describes the high-performance rotor blade design through the suitable combination of aerodynamic analysis, and efficient optimization technique to keep pace with this tendency.

Response surface method (RSM) is a collection of statistical and mathematical techniques useful for developing and improving the optimization process, which uses collectively design of experiment, regression analysis, and analysis of variance [9]. RSM has drawn much attention as an efficient and robust tool for multi-disciplinary design optimization (MDO) of aerospace vehicles [10, 11]. RSM is advantageous in MDO applications, since it provides the useful disciplinary models that can be easily combined with each other and be manipulated together by designers.

In this study, RSM is employed to the advanced hovering rotor design in subsonic and transonic conditions. The response surface models in regard to the rotor performance in two regimes are constructed using flow analysis, and genetic algorithm (GA) including objective functions and constraints is applied to accomplish the rotor airfoil design and the rotor tip shape design [12]. The influence of objective functions and constraints on rotor aerodynamic characteristics is also examined.

FLOW SOLVER

Three-dimensional Reynolds-averaged compressible Navier–Stokes equations are used to analyse the aerodynamic performance of the hovering rotor. Roe's flux difference splitting is used to discretize convective terms [13] and MUSCL with Koren limiter is applied for higher order spatial accuracy [14]. LU-SGS scheme is used to perform the time marching [15] and the algebraic Baldwin–Lomax model is adopted to take turbulence effects into account [16].

For validation, the aerodynamic calculations of the untwisted rectangular rotor blade with NACA 0012 airfoil are compared with experimental data [17]. A hyperbolic C-H-type grid system is applied, in which the grid size is $181 \times 53 \times 49$ in streamwise, radial, and perpendicular directions, respectively. The collective pitch of the test model is 8° and two operating conditions are used to simulate subsonic ($M_{\text{tip}} = 0.612$) and transonic ($M_{\text{tip}} = 0.877$) regimes. The prediction results of the pressure coefficient, C_p agree well with experimental data as shown in Figures 1 and 2.

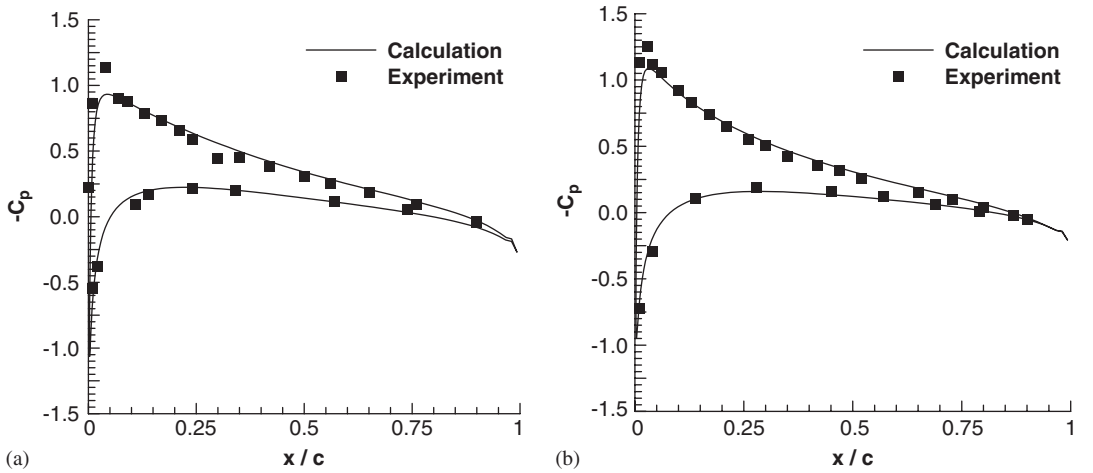

Figure 1. Comparison of C_p distribution: $\theta_c = 8°$, $M_{tip} = 0.612$: (a) spanwise location, $r/R = 0.80$; and (b) spanwise location, $r/R = 0.89$.

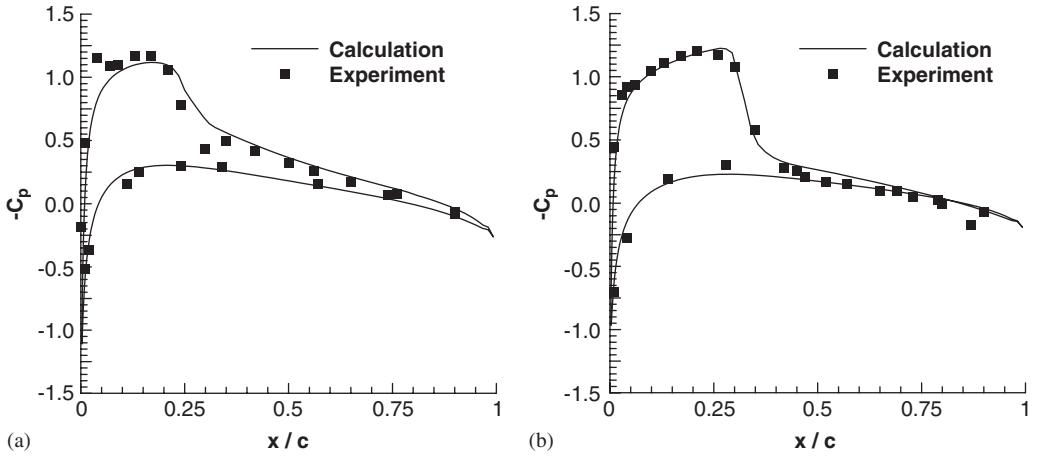

Figure 2. Comparison of C_p distribution: $\theta_c = 8°, M_{tip} = 0.877$: (a) spanwise location, $r/R = 0.80$; and (b) spanwise location, $r/R = 0.89$.

RESPONSE SURFACE METHOD

RSM builds a response model by calculating data points with experimental design theory to prescribe the response of a system with independent variables. The relationship can be written in a general form as follows:

$$y = F(x_1, x_2, \ldots, x_{n_v}) + \varepsilon \tag{1}$$

where ε represents the total error which is often assumed to have a normal distribution with zero mean. The response surface model, F is usually assumed as a second-order polynomial, which can be written for n_v design variables as follows:

$$y^{(p)} = c_0 + \sum_i c_i x_i + \sum_{1 \leqslant i \leqslant j \leqslant n_v} c_{ij} x_i x_j, \quad p = 1, \ldots, n_s \tag{2}$$

The above normal equations are expressed in a matrix form, $\mathbf{y} = X\mathbf{c}$ and the method of least squares is typically used to estimate the regression coefficients, $\mathbf{c}$ in a multiple linear regression model.

As a selection technique of data points, the 3-level factorial design with D-optimal condition is applied. D-optimal criterion states that the chosen data points are those that maximize the determinant, $|X^T X|$. D-optimal design is performed on the basis of Fedorov exchange algorithm developed by Alan Miller and Nam Nguyen from CSIRO, Melbourne, Australia.

Analysis of variance and regression analysis are the statistical techniques to estimate regression coefficients in the quadratic polynomial model and also yield a measure of uncertainty in the coefficients. One of the important statistical parameters is the coefficient of determination, R^2 which provides the summary statistic that measures how well the regression equation fits the data. It is given as

$$R^2 = \frac{\text{SSR}}{\text{SSTO}} = 1 - \frac{\text{SSE}}{\text{SSTO}} \tag{3}$$

where SSTO is the total sum of squares, SSR is the regression sum of squares, and SSE is the error sum of squares. From the inspection of Equation (3), it is found that $0 \leqslant R^2 \leqslant 1$. However, a large value of R^2 does not necessarily imply that the regression model is a good one. Adding a variable to the model always increases R^2, regardless of whether the additional variable is statistically significant or not. Thus, it is possible for the models that have large values of R^2 to yield the poor predictions of new observations or estimates of the mean response. Because R^2 always increases as we add terms to the model, the *adjusted*-R^2 statistic parameter, R^2_{adj} defined below is frequently used.

$$R^2_{\text{adj}} = 1 - \frac{\text{SSE}/(n_s - n_{rc})}{\text{SSTO}/(n_s - 1)} = 1 - \left(\frac{n_s - 1}{n_s - n_{rc}}\right)(1 - R^2) \tag{4}$$

In general, the *adjusted*-R^2 statistic does not always increase as variables are added to the model. In fact, if unnecessary terms are added, the value of R^2_{adj} often decreases.

It is important to determine the value of each regression variable in the regression model, because the model may be effective with the inclusion of additional variables or with the deletion of the variables already in the model. The test statistic (t-statistic) for testing the significance of any individual regression coefficient is

$$t = \frac{c_j}{\sqrt{\hat{\sigma}^2 C_{jj}}}, \quad j = 1, \ldots, n_{rc} \tag{5}$$

where $\hat{\sigma}^2$ is the estimation of variance and C_{jj} is the diagonal element of $(X^T X)^{-1}$ corresponding to c_j.

A genetic optimization code, GenocopIII (GEnetic algorithm for Numerical Optimization of COnstrained Problems III) developed by Michalewicz [18] is adopted in this study and the optimization process using RSM and GA is summarized in the flowchart given in Figure 3.

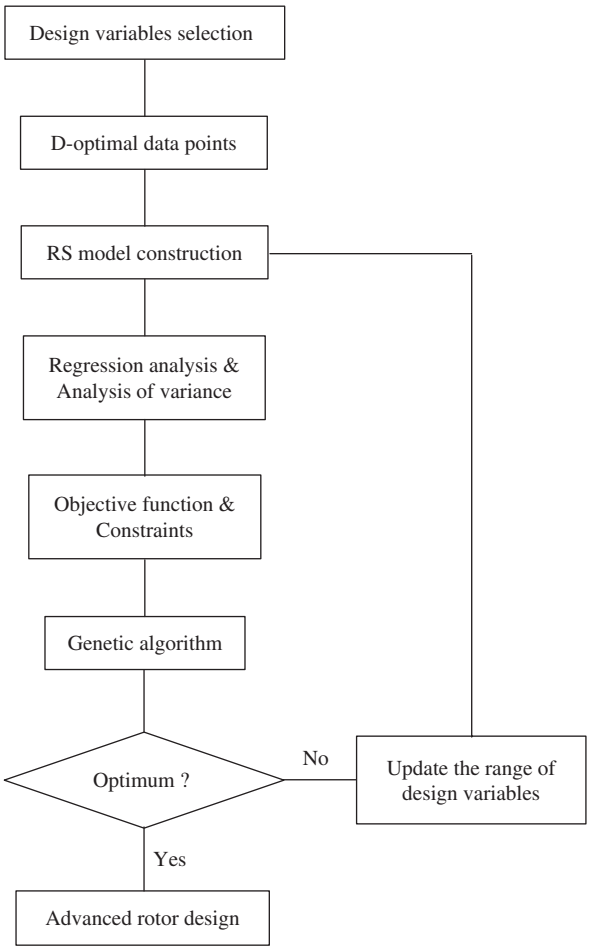

Figure 3. Optimization process flowchart.

RESULTS AND DISCUSSION

The optimization studies about the rotor airfoil design and the rotor blade design are accomplished to investigate the influence of design parameters on the hovering rotor performance in subsonic ($\theta_c = 10°$, $M_{tip} = 0.627$) and transonic ($\theta_c = 8°$, $M_{tip} = 0.821$) operating conditions. The influence of objective functions and constraints on the optimized rotor performance is also examined by four kinds of design problems, which are based on the combination of objective functions and constraints including thrust coefficient, torque coefficient, and Figure of Merit (Table I).

Airfoil design of rotor blade

The airfoil design of the rectangular rotor with $-8.35°$ linear twist and three airfoils (NPL9618, NPL9615, and NPL9617) is carried out. NPL9615 airfoil in $r/R = 0.85$ and NPL9617 airfoil in

Table I. Objective function and constraint for optimization process.

	Objective function	Constraint
Case 1	C_Q minimum	$C_T \geqslant (C_T)_{\text{baseline}}$
Case 2	F.M. maximum	$C_T \geqslant (C_T)_{\text{baseline}}$
Case 3	C_T maximum	$C_Q \leqslant (C_Q)_{\text{baseline}}$
Case 4	F.M. maximum	$C_Q \leqslant (C_Q)_{\text{baseline}}$

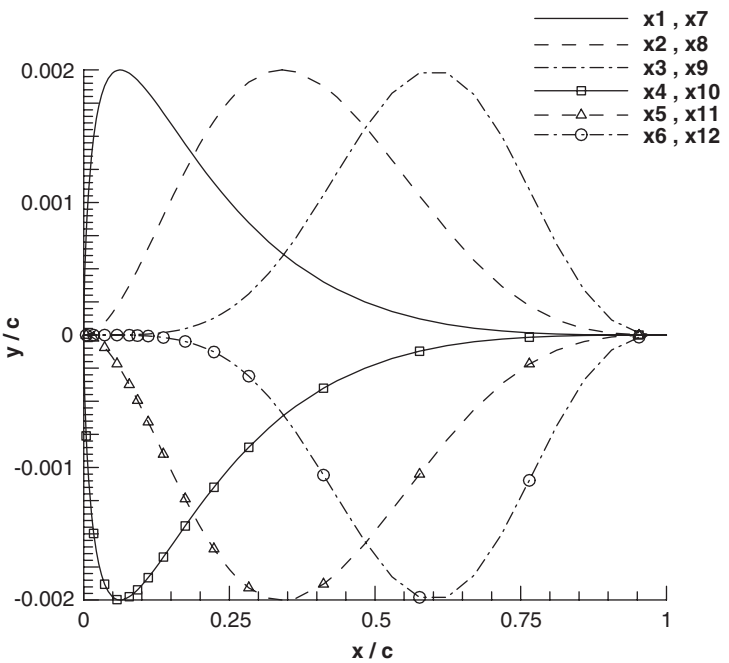

Figure 4. Shape function distribution.

$r/R = 1.0$ which constitute the rotor tip part are selected as baseline airfoils. The airfoil geometry is modified adding a linear combination of shape functions, f_k and weighting coefficients, w_k as follows [19]:

$$y = y_{\text{base}} + \sum_{k=1}^{n_v} w_k f_k$$
$$f_k = \sin^3[\pi x^{e(k)}], \quad e(k) = \frac{\ln(0.5)}{\ln(x_k)} \tag{6}$$

Twelve design variables are applied on both upper and lower sides of two airfoils, which have six shape parameters, respectively (x_1–x_6: NPL9615, x_7–x_{12}: NPL9617). The selected shape functions and boundaries of design variables are presented in Figure 4. To construct the quadratic response surface model, 183 numerical simulations and 91 regression coefficients are used.

It is necessary to estimate the accuracy of the response surface model, because it is the approximation model based on numerical results or experimental data. To do it, the fitting quality about rotor performance coefficients in two regimes is examined in Table II, and it proves that the aerodynamic characteristics depending on the airfoil shape change can be predicted accurately with the quadratic model. The t-statistic values are calculated to estimate the importance of design variables on the rotor aerodynamic performance prediction in Figure 5. The design variable of a higher t-statistic value has a more dominant effect on the response surface model. This implies that design results can be improved by increasing the variation range of dominant terms or by adding more design variables in the dominant region. The change of NPL9615 airfoil geometry has a more influence on thrust and torque coefficients. Especially, x_1 and x_7 terms, which are the design variables for modifying the upper surface close to the leading edge of two airfoils, have a higher t-statistic value in the transonic torque coefficient because of the shock-induced drag.

Because RSM enables the designer to modify objective functions and constraints easily during the optimization process, it is needed to examine the effect of various objective functions and constraints on the designed airfoil shape and the rotor performance. Based on four kinds of design problems in Table I, the convergence history of rotor performance coefficients by the genetic design combined with RSM is seen in Figure 7. Although the number of genetic evaluations is set to 20 000, the fast convergence to the optimal result makes an appearance because of the constraint condition. According to the comparison of the rotor performance by four kinds of design conditions (Figures 9 and 10), the design result of

Table II. Fitting quality in rotor airfoil design.

	Subsonic condition		Transonic condition	
	R^2	R^2_{adj}	R^2	R^2_{adj}
C_T	1.000	1.000	1.000	1.000
C_Q	0.999	0.998	0.999	0.998
F.M.	0.999	0.997	1.000	1.000

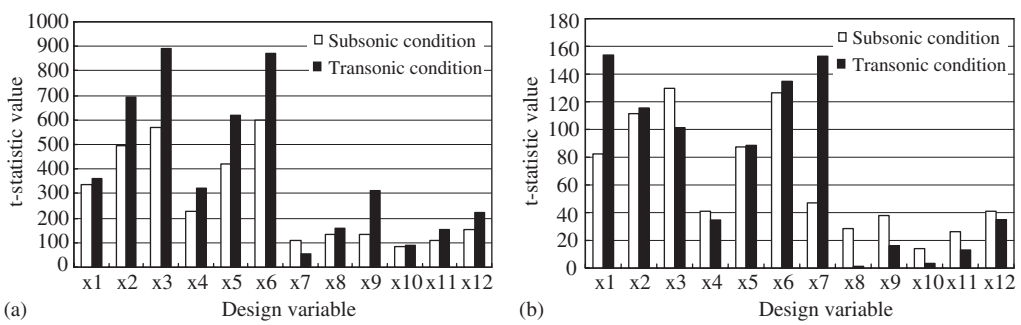

Figure 5. Comparison of t-statistic value in rotor airfoil design: (a) thrust coefficient; and (b) torque coefficient.

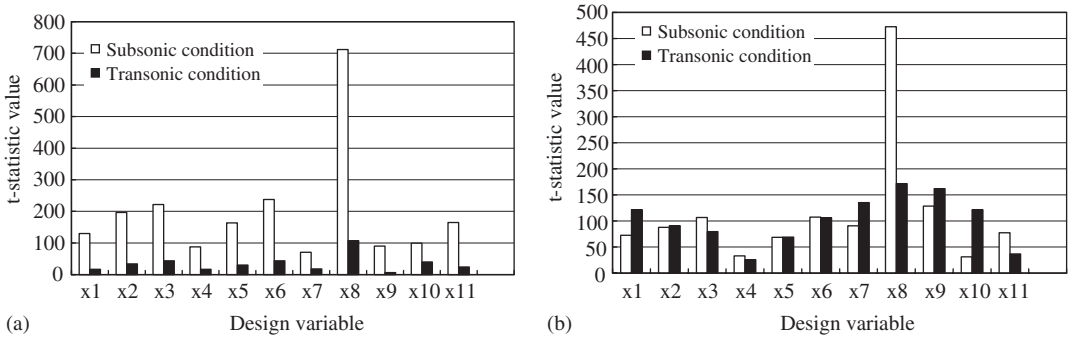

Figure 6. Comparison of t-statistic value in rotor blade design: (a) thrust coefficient; and (b) torque coefficient.

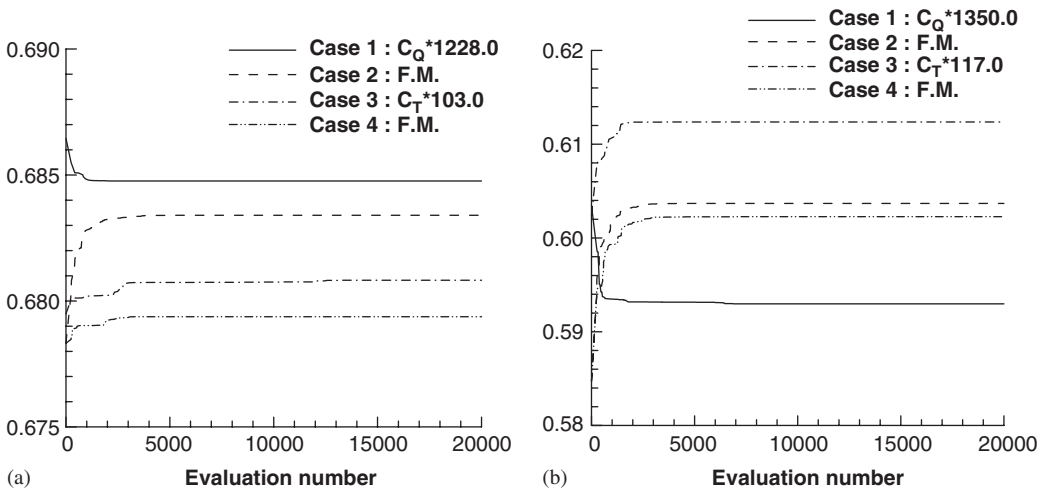

Figure 7. Convergence history of rotor airfoil design by RSM and GA (Case 1: C_Q minimum $+ C_T \geqslant (C_T)_{\text{baseline}}$, Case 2: F.M. maximum $+ C_T \geqslant (C_T)_{\text{baseline}}$, Case 3: C_T maximum $+ C_Q \leqslant (C_Q)_{\text{baseline}}$, Case 4: F.M. maximum $+ C_Q \leqslant (C_Q)_{\text{baseline}}$): (a) subsonic condition; and (b) transonic condition.

Case 2 shows the higher value of Figure of Merit, regardless of the torque coefficient increase. Moreover, the application of C_Q constraint (Cases 3 and 4) displays good results in the transonic design point. The various optimized airfoils are obtained using different objective functions and constraints in Figures 11 and 12. The airfoil geometry of Case 2 shows remarkable variations in the subsonic design and the change of reducing the thickness and modifying the leading edge shape is observed in the transonic design. These aspects reflect the results of the t-statistic distribution.

To find out multi-objectives capability, the dual-points design works covering subsonic and transonic regimes are performed. Among many approaches to solve multi-objective design

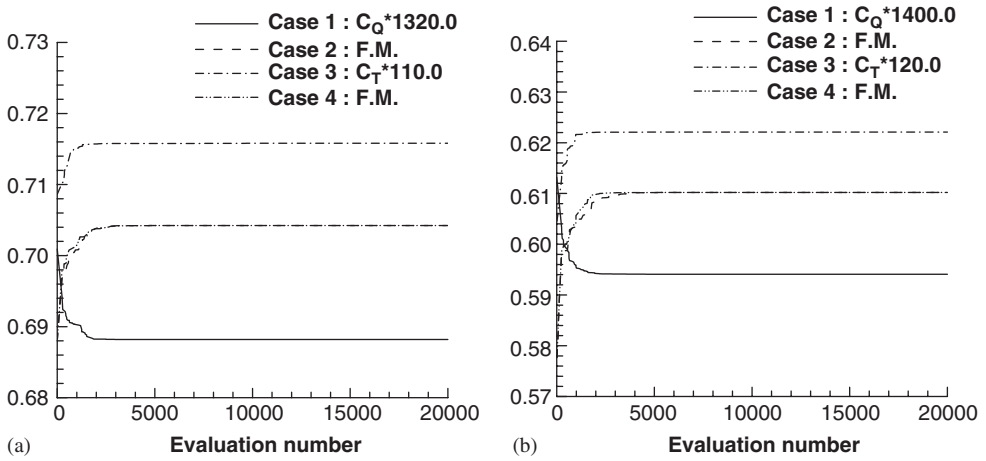

Figure 8. Convergence history of rotor blade design by RSM and GA (Case 1: C_Q minimum + $C_T \geqslant (C_T)_{\text{baseline}}$, Case 2: F.M. maximum + $C_T \geqslant (C_T)_{\text{baseline}}$, Case 3: C_T maximum+$C_Q \leqslant (C_Q)_{\text{baseline}}$, Case 4: F.M. maximum+$C_Q \leqslant (C_Q)_{\text{baseline}}$): (a) subsonic condition; and (b) transonic condition.

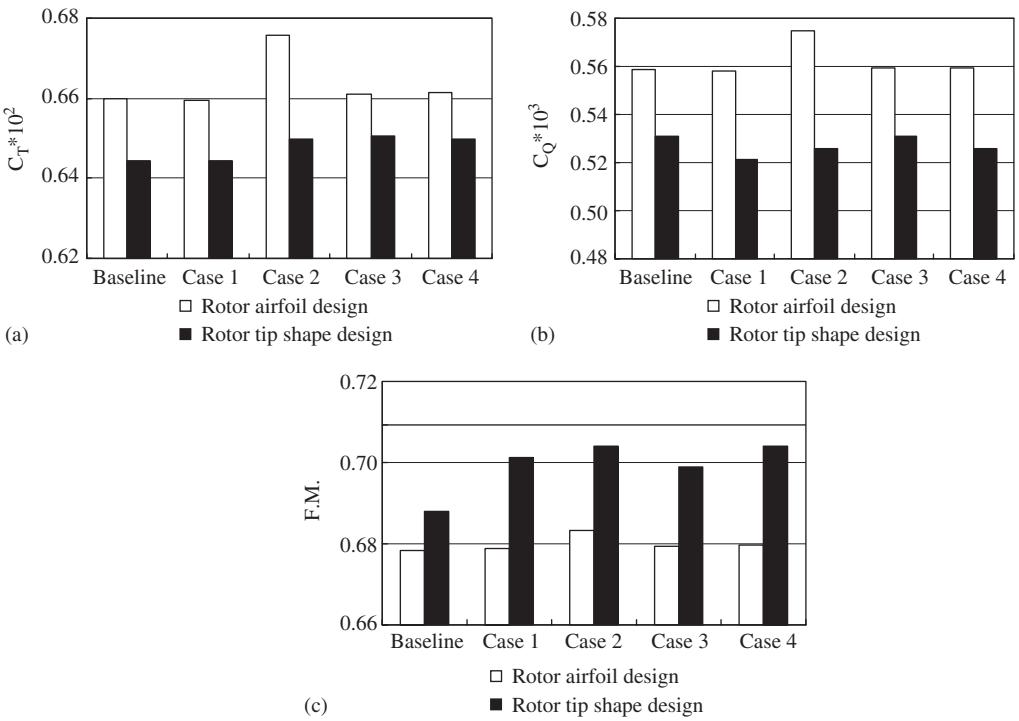

Figure 9. Comparison of rotor performance in subsonic condition (Case 1: C_Q minimum + $C_T \geqslant (C_T)_{\text{baseline}}$, Case 2: F.M. maximum + $C_T \geqslant (C_T)_{\text{baseline}}$, Case 3: C_T maximum + $C_Q \leqslant (C_Q)_{\text{baseline}}$, Case 4: F.M. maximum + $C_Q \leqslant (C_Q)_{\text{baseline}}$): (a) thrust coefficient; (b) torque coefficient; and (c) Figure of Merit.

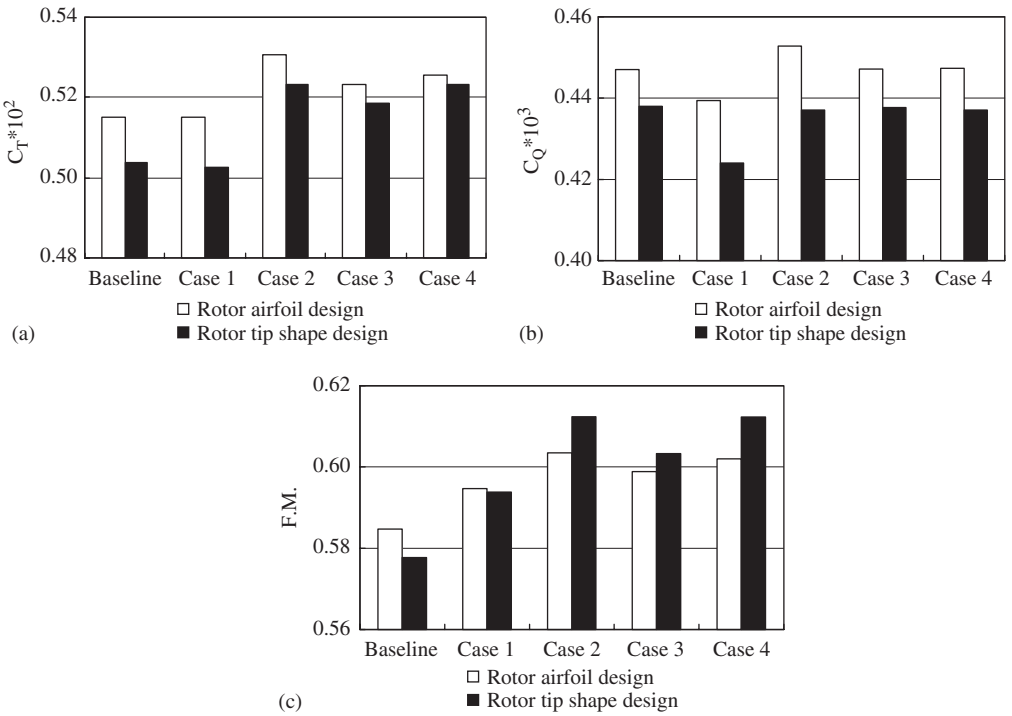

Figure 10. Comparison of rotor performance in transonic condition (Case 1: C_Q minimum $+ C_T \geqslant (C_T)_{\text{baseline}}$, Case 2: F.M. maximum $+ C_T \geqslant (C_T)_{\text{baseline}}$, Case 3: C_T maximum $+ C_Q \leqslant (C_Q)_{\text{baseline}}$, Case 4: F.M. maximum $+ C_Q \leqslant (C_Q)_{\text{baseline}}$): (a) thrust coefficient; (b) torque coefficient; and (c) Figure of Merit.

problems, the weighting objective method is used. This method takes each objective function and multiplies it by a fraction of one, the *weighting factor*, which is represented by we_j. The modified functions are then added together to obtain a single cost function. Mathematically, the new function is written as

$$f(X) = \sum_{j=1}^{k} \text{we}_j f_j(X), \quad 0 \leqslant \text{we}_j \leqslant 1, \ \sum_{j=1}^{k} \text{we}_j = 0 \tag{7}$$

To perform the dual-points design in subsonic and transonic conditions, the objective function with the weighting factor and constraints are selected below.

$$\text{Objective:} \quad \text{Minimize } \text{we} \times (C_Q)_{\text{Subsonic condition}} + (1 - \text{we}) \times (C_Q)_{\text{Transonic condition}}$$

$$\text{Subject to:} \quad (C_T)_{\text{Subsonic condition}} \geqslant (C_T)_{\text{Subsonic condition, baseline}} \text{ and}$$

$$(C_T)_{\text{Transonic condition}} \geqslant (C_T)_{\text{Transonic condition, baseline}} \tag{8}$$

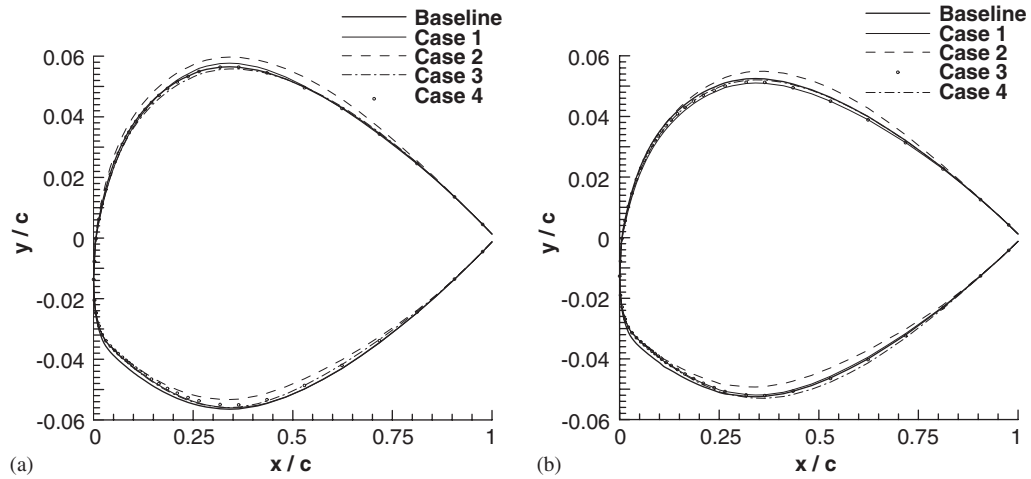

Figure 11. Comparison of airfoil geometry in subsonic condition: rotor airfoil design (Case 1: C_Q minimum$+C_T \geqslant (C_T)_{\text{baseline}}$, Case 2: F.M. maximum$+C_T \geqslant (C_T)_{\text{baseline}}$, Case 3: C_T maximum$+C_Q \leqslant (C_Q)_{\text{baseline}}$, Case 4: F.M. maximum$+C_Q \leqslant (C_Q)_{\text{baseline}}$): (a) NPL9615 airfoil; and (b) NPL9617 airfoil.

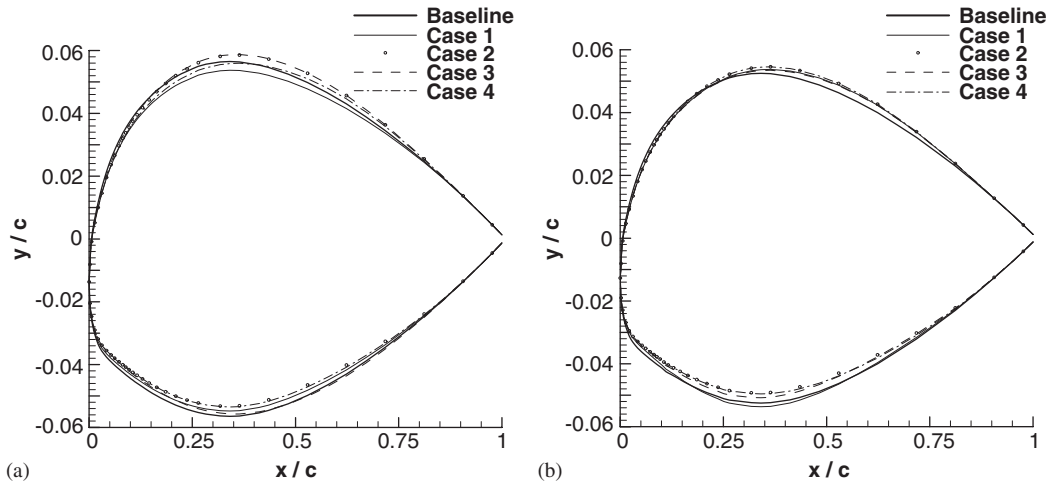

Figure 12. Comparison of airfoil geometry in transonic condition: rotor airfoil design (Case 1: C_Q minimum$+C_T \geqslant (C_T)_{\text{baseline}}$, Case 2: F.M. maximum$+C_T \geqslant (C_T)_{\text{baseline}}$, Case 3: C_T maximum$+C_Q \leqslant (C_Q)_{\text{baseline}}$, Case 4: F.M. maximum$+C_Q \leqslant (C_Q)_{\text{baseline}}$): (a) NPL9615 airfoil; and (b) NPL9617 airfoil.

Figures 15 and 16 display the variations of the rotor aerodynamic performance according to the weighting factor. The thrust coefficient of the subsonic region is severely restricted by the constraint condition in contrast with that of the transonic region and the improvement of rotor aerodynamic characteristics in the transonic condition is remarkable.

Tip shape design of rotor blade

The blade tip shape design includes the effect of eleven geometrical parameters, which are composed of airfoil shape (x_1–x_6), tip twist (x_7), tip chord (x_8), tip sweep (x_9), tip anhedral (x_{10}), and initiation point of taper, sweep, anhedral (the same position, x_{11}). The airfoil geometry has the same shape functions and design ranges as the airfoil design case and Table III indicates the detailed information of rotor blade design variables. To construct the quadratic response surface model, 157 numerical simulations and 78 regression coefficients are used.

The rotor airfoil design procedure shows the importance of NPL9615 airfoil shape, because it plays a more part in the rotor performance. For this reason, the rotor shape design includes the change of NPL9615 airfoil geometry. The fitting quality results of the response surface model present a good accuracy, regardless of many design variables and the shock-induced non-linear effect in the transonic condition (Table IV). Figure 6 exhibits the influence of rotor shape design variables on the rotor performance in two regimes. The relative contribution of the rotor airfoil geometry and the planform shape makes a little difference with the exception of the remarkable chord effect, which is closely related to the rotor blade area and the aerodynamic characteristics by the change of Reynolds number. In the torque coefficient of the transonic condition, it is observed that the design variables including the leading edge part of the airfoil geometry and the rotor shape are important from the viewpoint of transonic rotor flow characteristics.

The convergence history of rotor performance coefficients by GA is seen in Figure 8, and the genetic designs with the objective function of F.M. maximum (Cases 2 and 4) have the similar optimum value of Figure of Merit. The design results based on four kinds of design conditions are compared with the baseline rotor performance in Figures 9 and 10, and show the

Table III. Range of rotor blade design variable.

Design variable	Lower value	Baseline value	Upper value
Blade geometry			
Linear twist (deg)	−9.35	−8.35	−7.35
Tip chord (mm)	32.92	42.92	52.92
(Taper ratio)	(2.0)	(1.53)	(1.24)
Tip sweep (deg)	0.0	5.0	10.0
Tip anhedral (deg)	0.0	5.0	10.0
Initiation point (r/R) of taper, sweep, anhedral	0.89	0.9	0.91

Table IV. Fitting quality in rotor blade design.

	Subsonic condition		Transonic condition	
	R^2	R^2_{adj}	R^2	R^2_{adj}
C_T	1.000	1.000	0.997	0.993
C_Q	1.000	1.000	0.999	0.999
F.M.	0.999	0.999	0.995	0.991

improvement of Figure of Merit caused by the double effect of the torque coefficient reduction and the thrust coefficient increase. The advanced airfoils are obtained by the variation of the camber and thickness distribution and their geometries reflect the t-statistic distribution well (Figures 13 and 14). Tables V and VI present the optimized rotor shapes of two hovering conditions. The increase of linear twist and anhedral corresponds to the fact that high blade twist and anhedral produce the good hovering performance. The chord reduction of the subsonic design results in improving the rotor performance by unloading the tip part, and the chord increase of the transonic design has the advantage of advancing aerodynamic characteristics by high Reynolds number. The sweep effect is shown in Case 3 of the subsonic design, and the proper application of sweep and initiation point in Case 1 of the transonic design produces the good result of decreasing the shock-induced torque by reducing the compressibility effect. Through the geometry comparison of optimized rotor blades, it is observed that the design values of optimized rotor blades are adequately arranged to progress the rotor hovering performance according to the design problems.

In the manner of the rotor airfoil design, the dual-points design of the rotor shape is performed to consider the multi-objectives effect. Through the rotor performance distribution by the weighting factor change in Figures 15 and 16, the subsonic thrust coefficient satisfies the constraint condition. When the weighting factor increases (the subsonic design has a relative importance), Figure of Merit in the transonic condition shows small variations due to the augmentation of thrust and torque coefficients.

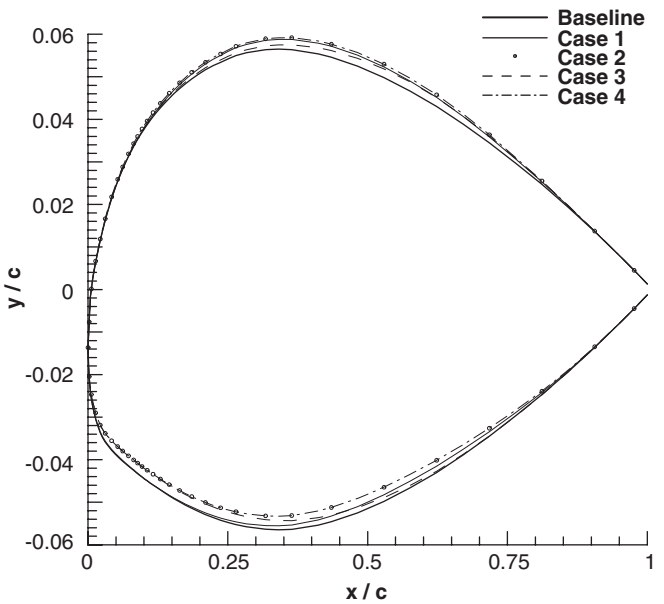

Figure 13. Comparison of NPL9615 shape in subsonic condition: rotor blade design (Case 1: C_Q minimum $+ C_T \geqslant (C_T)_{\text{baseline}}$, Case 2: F.M. maximum $+ C_T \geqslant (C_T)_{\text{baseline}}$, Case 3: C_T maximum $+ C_Q \leqslant (C_Q)_{\text{baseline}}$, Case 4: F.M. maximum $+ C_Q \leqslant (C_Q)_{\text{baseline}}$).

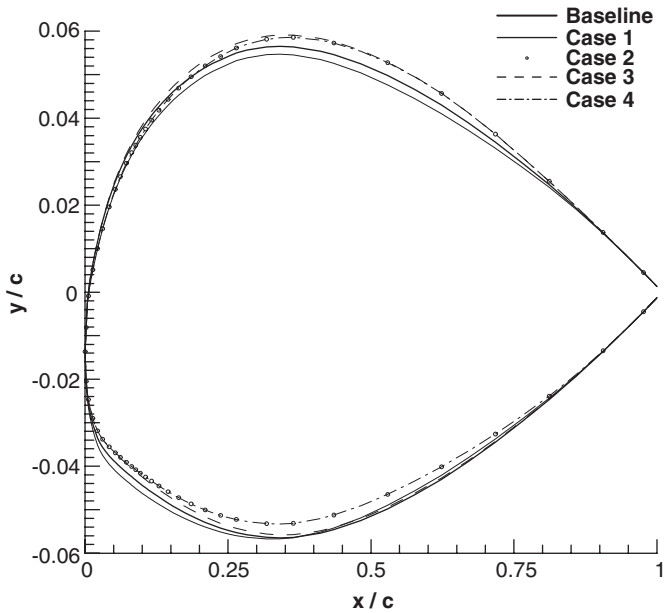

Figure 14. Comparison of NPL9615 shape in transonic condition: rotor blade design (Case 1: C_Q minimum + $C_T \geqslant (C_T)_{\text{baseline}}$, Case 2: F.M. maximum + $C_T \geqslant (C_T)_{\text{baseline}}$, Case 3: C_T maximum + $C_Q \leqslant (C_Q)_{\text{baseline}}$, Case 4: F.M. maximum + $C_Q \leqslant (C_Q)_{\text{baseline}}$).

Table V. Optimized blade geometry of subsonic design.

Design variable	Baseline	Case 1	Case 2	Case 3	Case 4
Linear twist (deg)	−8.35	−9.35	−9.35	−9.35	−9.35
Tip chord (mm)	42.92	34.96	32.92	39.46	32.92
(Taper ratio)	(1.53)	(1.88)	(2.0)	(1.67)	(2.0)
Tip sweep (deg)	5.0	0.32	0.0	4.02	0.0
Tip anhedral (deg)	5.0	10.0	10.0	10.0	10.0
Initiation point (r/R) of taper, sweep, anhedral	0.9	0.9011	0.91	0.9094	0.91

Table VI. Optimized blade geometry of transonic design.

Design variable	Baseline	Case 1	Case 2	Case 3	Case 4
Linear twist (deg)	−8.35	−9.35	−9.35	−8.94	−9.35
Tip chord (mm)	42.92	45.13	49.36	48.48	49.31
(Taper ratio)	(1.53)	(1.46)	(1.33)	(1.36)	(1.34)
Tip sweep (deg)	5.0	3.64	0.0	0.87	0.0
Tip anhedral (deg)	5.0	10.0	10.0	10.0	10.0
Initiation point (r/R) of taper, sweep, anhedral	0.9	0.8915	0.91	0.9078	0.91

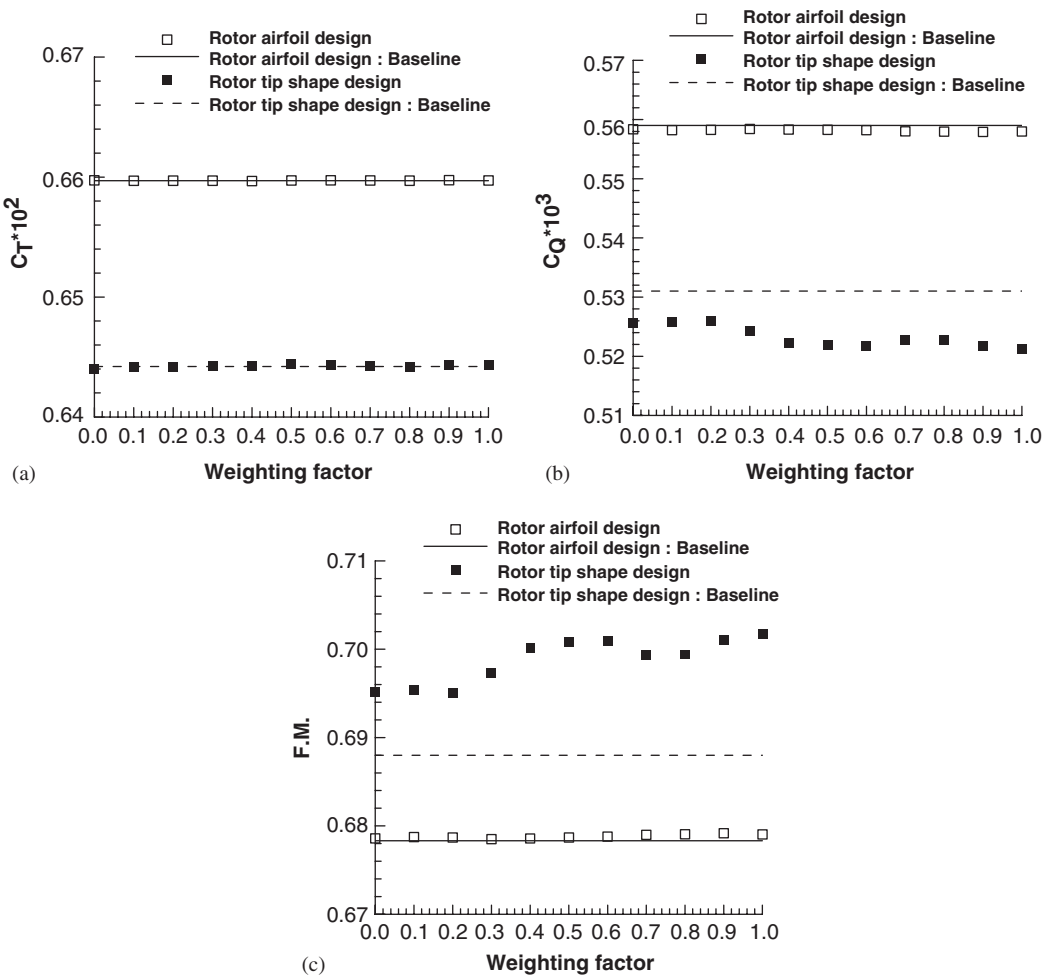

Figure 15. Rotor performance versus weighting factor in subsonic condition (we: weighting factor, we $\times$ $(C_Q)_{\text{Subsonic condition}}$ + (1 − we) $\times$ $(C_Q)_{\text{Transonic condition}}$ minimum + $(C_T)_{\text{Subsonic condition}} \geqslant (C_T)_{\text{Subsonic condition, baseline}}$ and $(C_T)_{\text{Transonic condition}} \geqslant (C_T)_{\text{Transonic condition, baseline}}$): (a) thrust coefficient; (b) torque coefficient; and (c) Figure of Merit.

CONCLUDING REMARKS

The present work is focused on introducing an efficient and robust optimization method to develop the advanced rotor blade in various hovering conditions. The design procedure including RSM and GA is combined with Navier–Stokes flow analysis and the statistical approach is used to guarantee the accuracy of the optimization design. The *t*-statistic values are calculated to give a more information about the influence of design variables on the rotor hovering performance. The advanced rotor geometry and the improved rotor performance are obtained from the rotor airfoil design and the rotor tip shape design. Although RSM has a limitation on the number

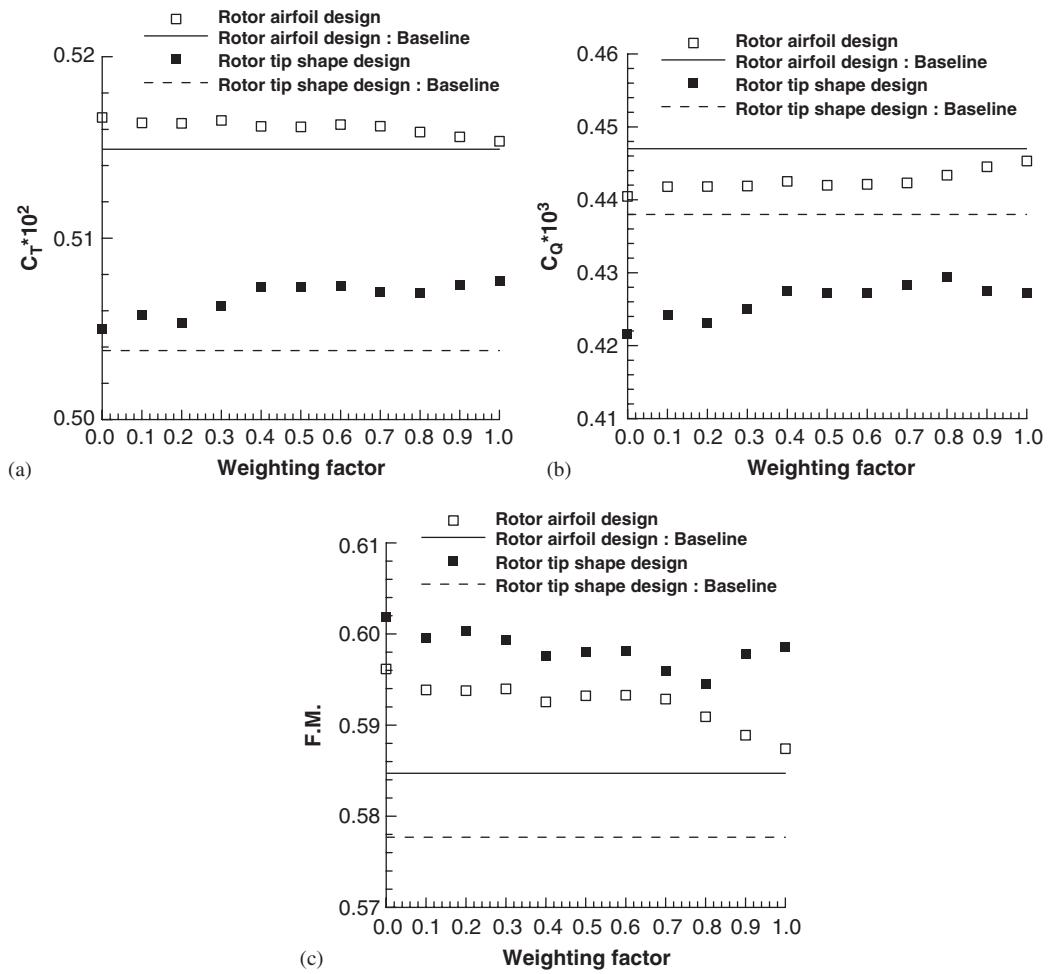

Figure 16. Rotor performance versus weighting factor in transonic condition (we: weighting factor, we $\times$ $(C_Q)_{\text{Subsonic condition}} + (1 - \text{we}) \times (C_Q)_{\text{Transonic condition}}$ minimum $+ (C_T)_{\text{Subsonic condition}} \geqslant (C_T)_{\text{Subsonic condition, baseline}}$ and $(C_T)_{\text{Transonic condition}} \geqslant (C_T)_{\text{Transonic condition, baseline}}$): (a) thrust coefficient; (b) torque coefficient; and (c) Figure of Merit.

of design variables due to the computational cost and the range of design variables is a little narrow because of the response surface model accuracy, this technology is a viable optimization tool for the rotor aerodynamic design.

NOMENCLATURE

c	chord length
c_0, c_i, c_{ij}	regression coefficients
C_T	thrust coefficient

C_Q	torque coefficient
F.M.	Figure of Merit: the ratio of the induced power (the power required to produce the rotor thrust) to the actual power
$f(X)$	objective function
M_{tip}	hovering tip Mach number
n_{rc}	number of regression coefficients
n_{s}	number of observations
n_{v}	number of design variables
r/R	radial location
X	$n_{\text{s}} \times n_{\text{rc}}$ matrix
x	independent variable
y	response variable
$\mathbf{y}$	response variable vector
θ_{c}	collective pitch

Subscripts

baseline	baseline rotor blade
base	baseline airfoil

Superscripts

T	transpose

ACKNOWLEDGEMENTS

The authors acknowledge the support for this research work by Ministry of Science and Technology in Korea, and Korea Aerospace Research Institute (KARI) through National Research Laboratory (NRL) Program.

REFERENCES

1. Mcveigh MA, Mchugh FJ. Influence of tip shape, chord, blade number, and airfoil on advanced rotor performance. *Journal of the American Helicopter Society* 1984; **29**(4).
2. Joanne LW, Katherine CY, Jocelyn IP, Howard MA, Wayne M. Multilevel decomposition approach to integrated aerodynamic/dynamic/structural optimization of helicopter rotor blades. *Presented at AHS Aeromechanics Specialists Conference*, San Francisco, CA, 1994.
3. Miura H. Application of numerical optimization methods to helicopter design problems: a survey. *NASA TM 86010*, 1984.
4. Bennett RL. Application of optimization methods to rotor design problems. *Vertica* 1983; **7**(3).
5. Nixon MW. Preliminary structural design of composite main rotor blades for minimum weight. *NASA TP 2730*, 1987.
6. Friedmann PP, Shantakumaran P. Optimum design of rotor blades for vibration reduction in forward flight. *Proceedings of the 39th Annual Forum of the AHS*, Saint Louis, MO, 1983.
7. Adelman HM, Mantay WR. Integrated multidisciplinary optimization of rotorcraft: a plan for development. *NASA TM 101617*, 1989.
8. Adelman HM, Mantay WR. Integrated multidisciplinary optimization of rotorcraft. *Journal of Aircraft* 1991; **28**(1):22–28.
9. Myers RH, Montgomery DC. *Response Surface Methodology*: *Process and Product Optimization Using Designed Experiments*. Wiley: New York, 1995.

10. Sobieszczanski-Sobieski J, Haftka RT. Multi-disciplinary aerospace design optimization: survey of recent development. *AIAA Paper No. 96-0711*, 1996.
11. Ahn J, Kim H, Lee D, Rho O. Response surface method for airfoil design in transonic flow. *Journal of Aircraft* 2001; **38**(2):231–238.
12. Goldberg DE. *Genetic Algorithms in Search*, *Optimization and Machine Learning*. Addison-Wesley: Reading, MA, 1989.
13. Roe PL. Approximate Riemann solvers, parameter vectors, and difference schemes. *Journal of Computational Physics* 1981; **43**(3):357–372.
14. Sweby PK. High resolution TVD schemes using flux limiters. *Lectures in Applied Mathematics* 1985; **22**.
15. Jameson A, Yoon S. Lower–upper implicit schemes with multiple grids for the Euler equations. *AIAA Journal* 1987; **25**:929–935.
16. Baldwin BS, Lomax J. Thin layer approximation and algebraic model for separated turbulent flows. *AIAA Paper 78-0257*, 1978.
17. Caradonna FX, Tung C. Experimental and analytical studies of a model helicopter rotor in hover. *NASA TM 81232*, 1980.
18. Michalewicz Z. *Genetic Algorithm + Data Structures = Evolutionary Programs*. Springer: New York, 1992.
19. Hicks RM, Henne PA. Wing design by numerical optimization. *Journal of Aircraft* 1978; **15**(7):407–412.

